LUNEBERG LENS SIMULATION IN A RIPPLE TANK

N. L. Walbridge and L. A. Woodward
University of Vermont

(Sponsored by the Office of Naval Research)

During the past four years a group at the University of Vermont Physics and Electrical Engineering Departments have developed the ripple tank as a quantitative tool. By optical means, using a coincidence of two line images from certain sections of neighboring waves, amplitudes of small ripples within a 30 d.b. intensity range are measured with accuracies approaching two percent.

In the Proceedings of 1955 we reported briefly on the use of the ripple tank. Index simulation is accomplished by thin layers of water over blocks of transparent material. The reduced speed of ripples in shallow water produces shorter wavelengths and the effects of refraction.

We have now extended the range of index values to more than two, corresponding to dielectric constants over four. The attenuation due to absorption is larger than for the case of radar, and it also increases faster with index. This should not, however, prevent the successful simulation of many radar actions.

A recent application has been the simulation of the Luneberg lens in which the dielectric of a sphere must vary as $(2-r^2)$ from the center out to the surface where $r = 1$. For the ripple tank a circular disk about eight wavelengths in diameter was machined down to a dome-like shape so that the depth of water over any point was such as to give an index value according to the above definition.

Figure 1 is a representation of the radiation produced by this disk lens with a point source on the rim. The absorption through the center part of the lens is seen to have reduced the power in the center of the beam. The phase fronts, however, are substantially straight lines. This particular simulation is not perfect, due in part to the difficulty of machining the slight change in cut over the surface of the disk.

In order to avoid the effect of the larger absorption through the center of the lens, and also to conform with actual radar practice, the point source was replaced by a directed beam. This was given by a sectoral horn simulation, with a half-power beam width of 16°.

The effective or virtual center of this primary radiation was some distance from the rim of the lens, that is, it was outside the focus. The resulting radiation is seen in Figure 2. Something of an image is produced a short distance from the lens, toward which the emergent waves first converge and from which they then diverge.

In order to move back the focal point from the rim of the lens to the position of the feed pattern source, that is, to reduce the refracting power of the lens, the index was reduced over the entire disk. This was accomplished by raising the water level slightly by adding a measured amount of water to the tank. This was only one arbitrary, but a very convenient, way of decreasing the index at every point. Since this is a departure from the theoretical index distribution of the Luneberg lens, there are probably many other distributions which would be usable. The most desirable one would probably be obtained only by experiment.

Figure 3 shows the main lobe of the radiation produced after several trials of adding slight amounts of water. It consists of practically "plane" waves. The beam shape is smooth, similar to that from a small reflector, and has a half-power beam width of the order of six degrees.

The next point considered was the fact that any radar lens of this type has to be constructed of shells of chosen thickness and appropriate dielectric to approximate as closely as possible the theoretical variation. We then simulated such lenses by machining disks to various discreet levels. Choice of index steps was arbitrary and the number of such steps was varied from five to ten.

The result of one such adaptation is shown in Figure 4, with hardly any basis for choosing between this and the preceding figure. Only five steps of index variation and corresponding thickness of rings (instead of shells) were used.

Curves of the radiation pattern above and also for three other slightly different water levels over this five-step lens are plotted in Figure 5. All intensity values were normalized to the same maximum value. These were measured at a radial distance of twelve or more wavelengths from the lens, which may, perhaps, be considered as in far field.

All of these curves show the same general smooth shape, with half-power beam widths from 5.8° to 7.0°. These seem to show that a satisfactory beam may be produced by a smaller number of shells of discreet dielectric values than might be supposed. Also, the assortment of dielectric constants required may not be critical. Those most available could be selected and the thicknesses determined accordingly. In these examples given here no measurements of the index values were made. More work would relate beam shape and width to specific and practical designs of such lenses.

Side lobes with these small aperture lens simulations are very low. Measurements have not yet been made on them, but they seem to be of the order of 20 d.b. down from the peak intensity.

Another project for investigation is illustrated in Figure 6. By inserting a simulated section of a radome wall into a beam, the boresight shift caused thereby can be measured to perhaps a half mil. By varying the angle of incidence a curve could be obtained giving the boresight shift at all aspects of a given radome shape with a specified antenna location. Other curves would show the effect of wall thickness and dielectric constant since these can be simulated over sufficiently wide ranges. The probability seems good that a combination of these parameters can be found that will produce a boresight shift constant over the angle of look.

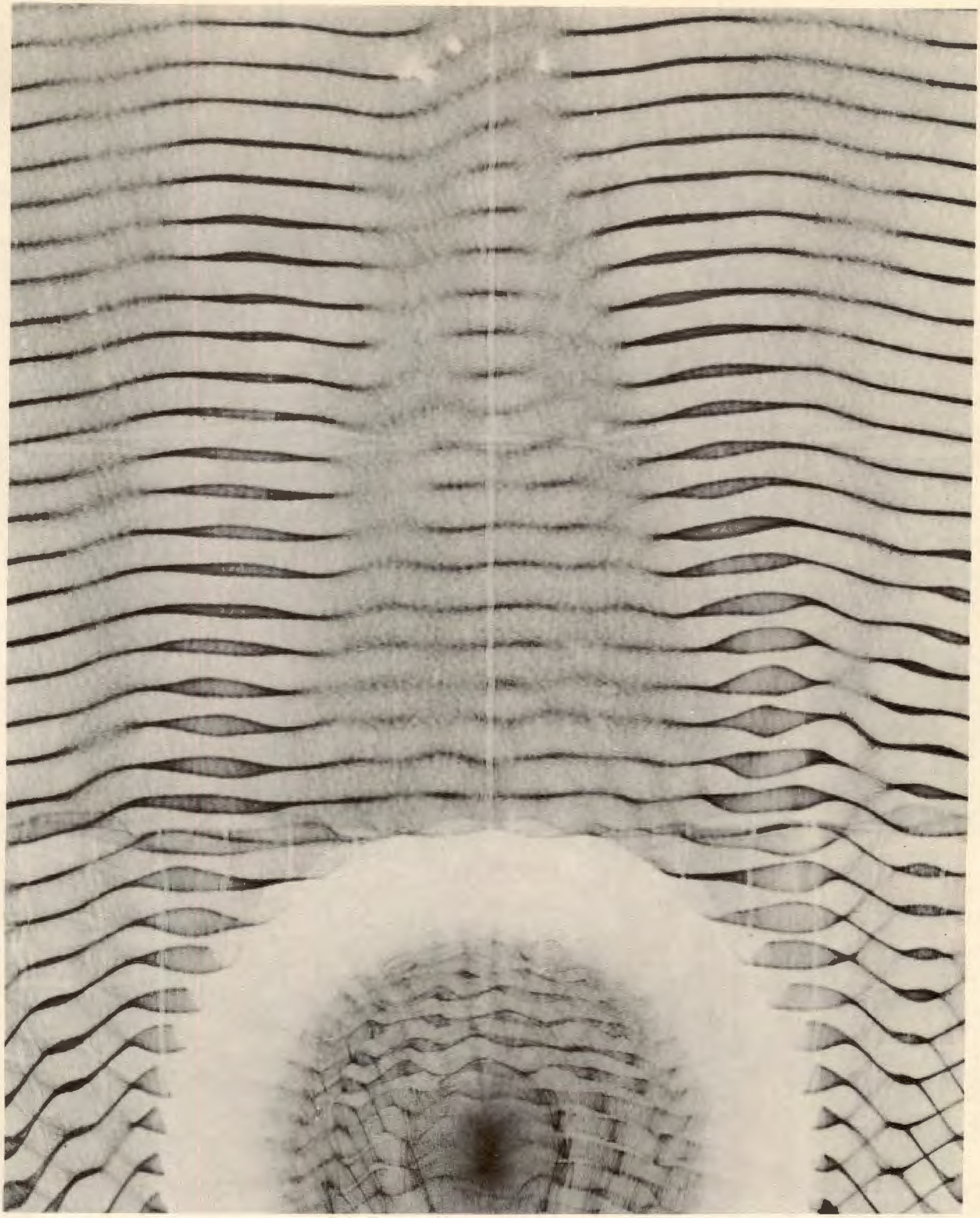

Fig. 1. Luneberg Lens Simulated by Machined Contour under Water.

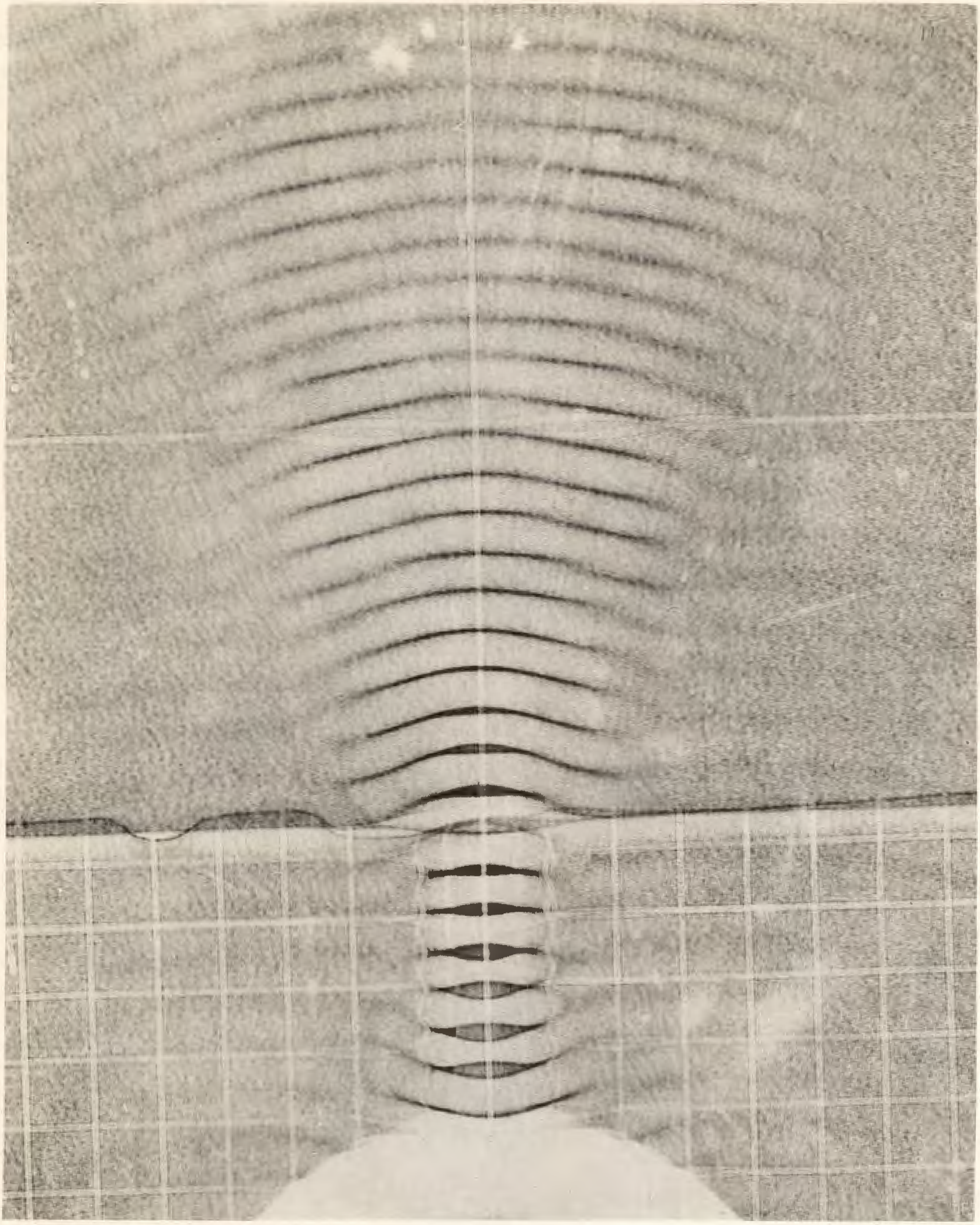

Fig. 2. Luneberg Lens with Horn Feed, Center of Feed Some Distance from Lens.

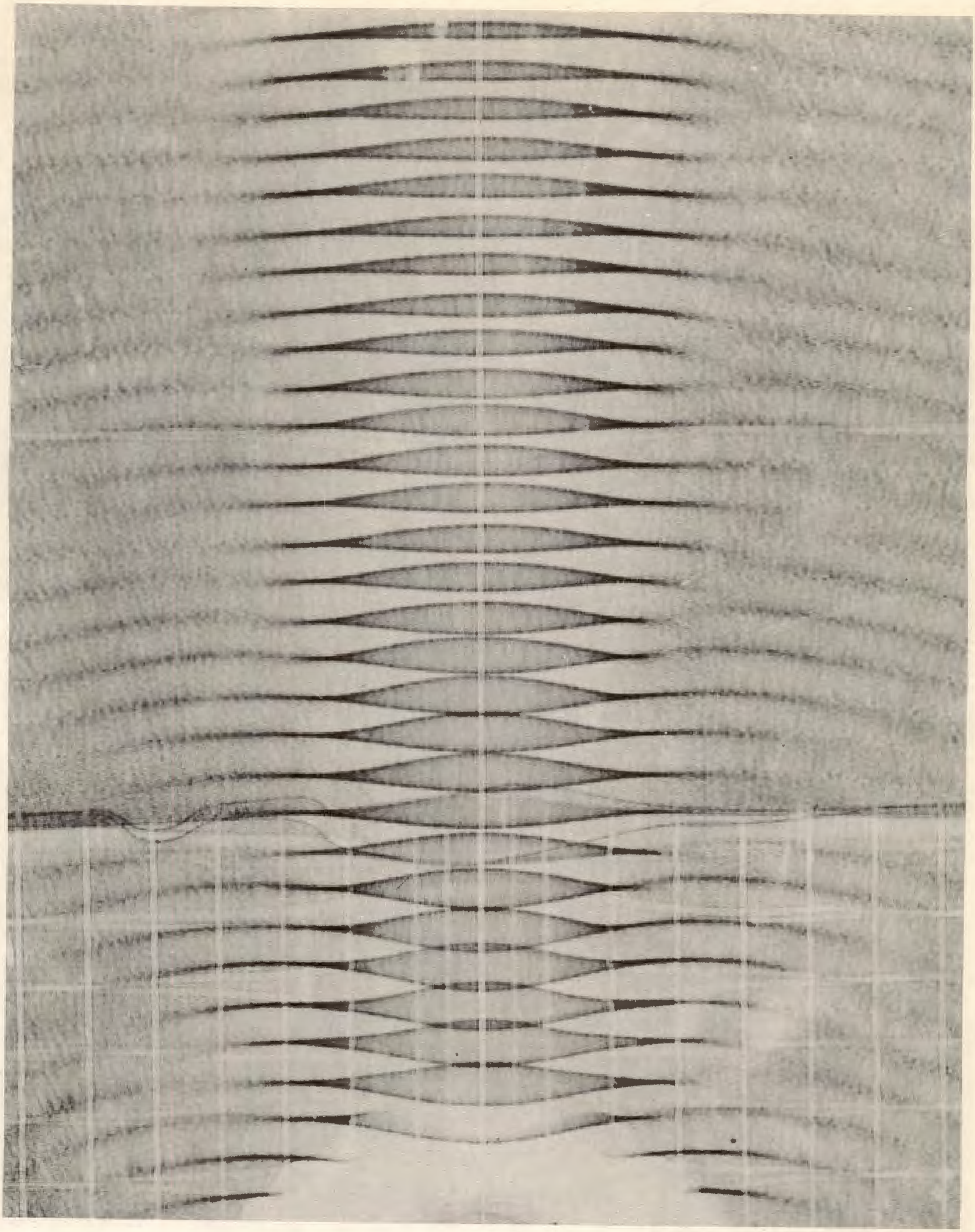

Fig. 3. Same as Fig. 2, with Index at All Points Reduced Slightly.

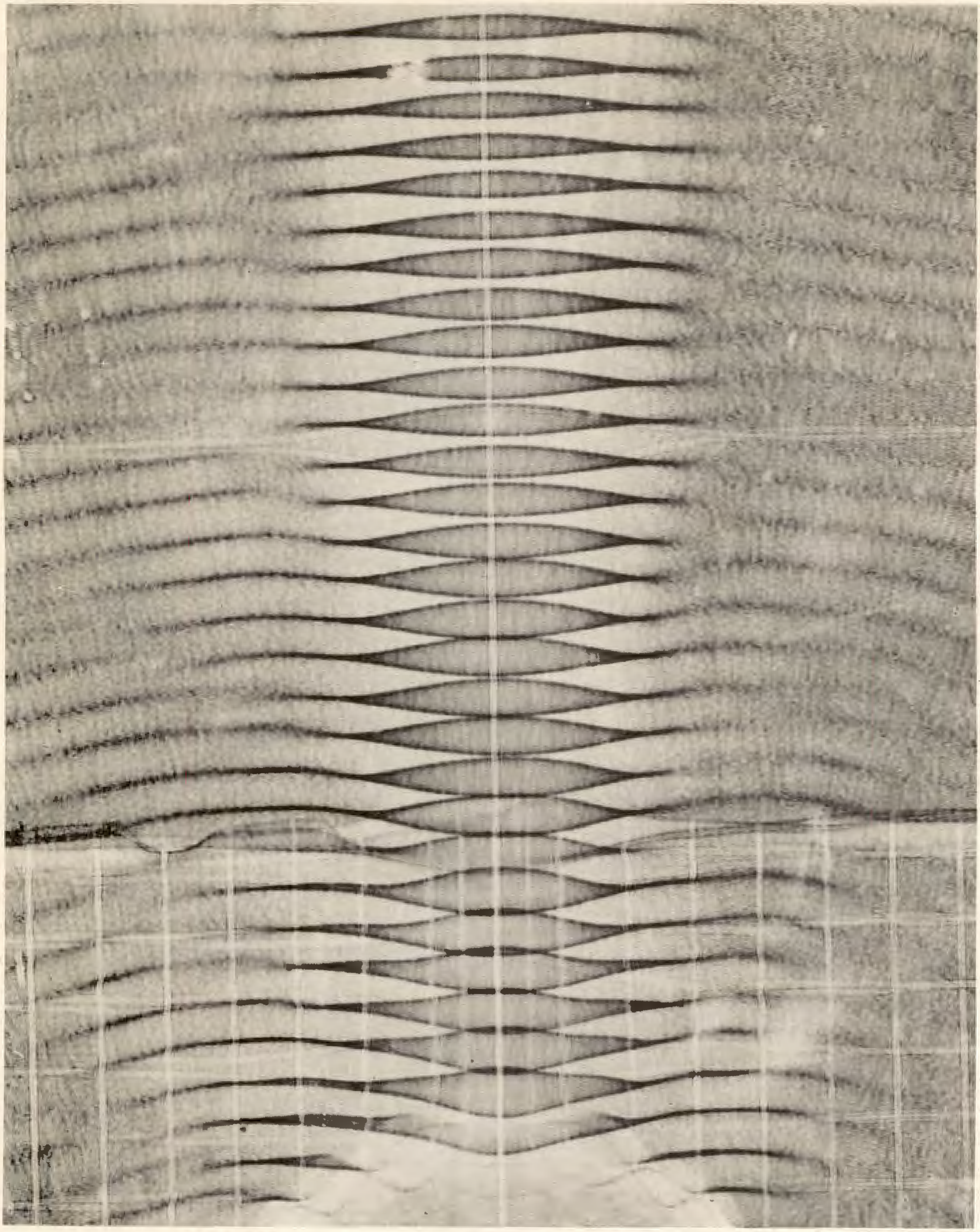

Fig. 4. Modified Luneberg Lens Consisting of Five Shells.
(Cf. Fig. 3)

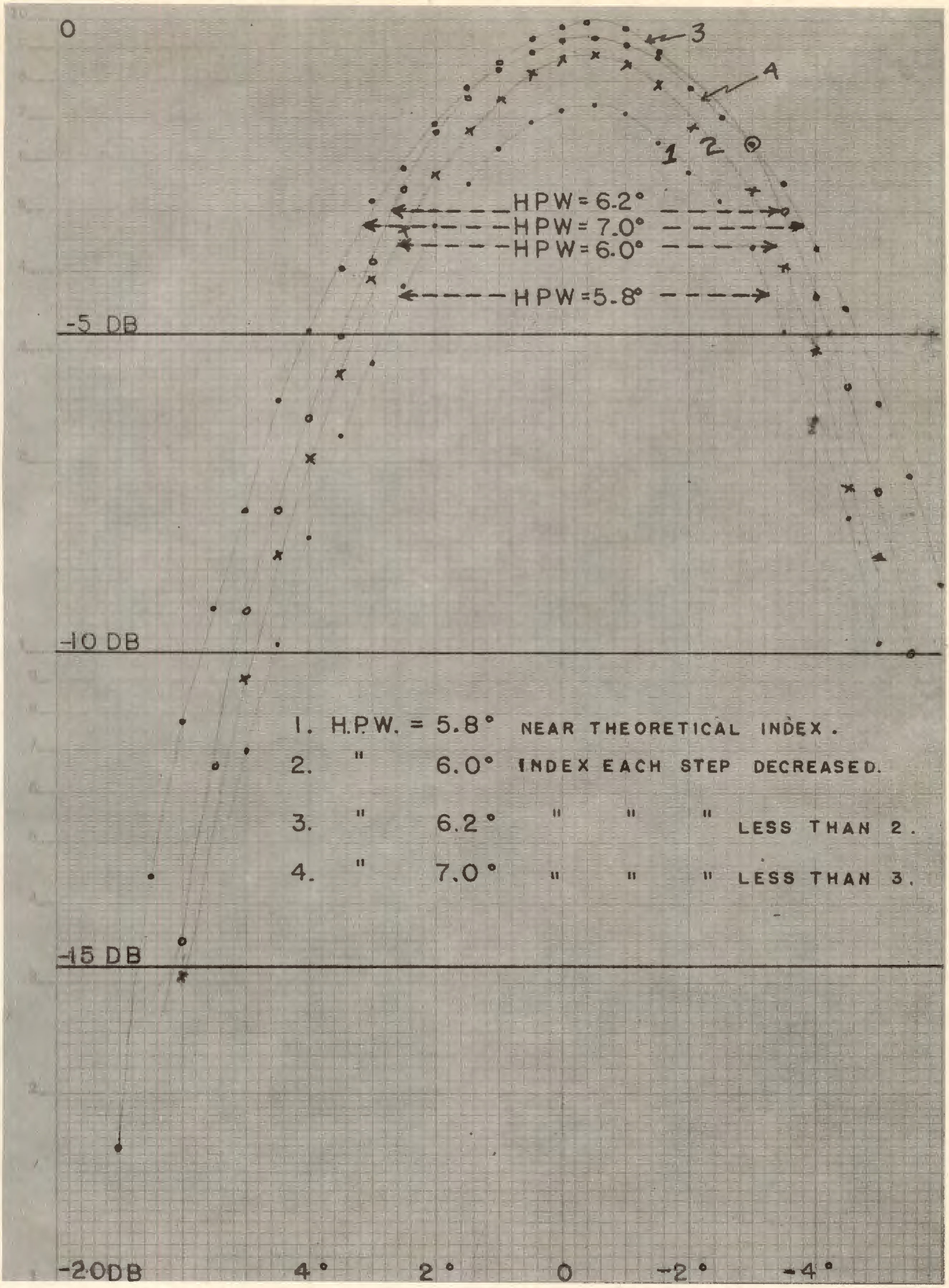

Fig. 5. Curves of Pattern in Fig. 4 with Three Other Index Variations over Same Lens.

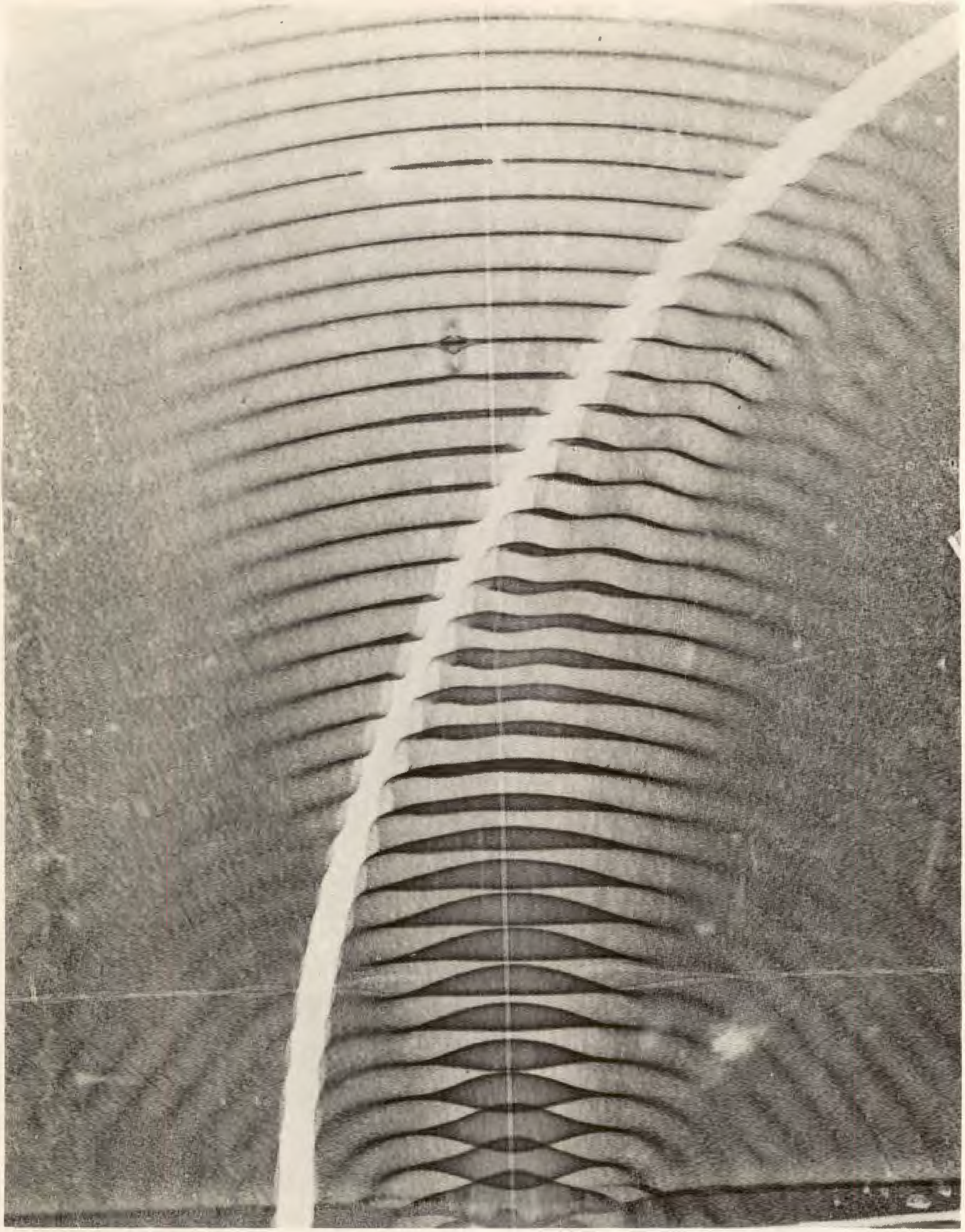

Fig. 6. Boresight Shift Due to Section of Radome Wall Can Be Measured.

over sufficiently wide ranges. The probability seems good that a combination of these parameters can be found that will produce a boresight shift constant over the angle of look.